Supporting Information

Supramolecular interaction facilitated small molecule films for organic field effect transistors

Arulraj ArulKashmir, Rajashree Y. Mahale, Satej S. Dharmapurikar, Manoj K. Jangid and Kothandam Krishnamoorthy*

Experimental Section

Poly(4-vinyl pyridine) and Zinc (II) porphyrin were purchased from Aldrich chemicals and used as received. The chloroform was also purchased from Aldrich and then vacuum distilled before use. UV-vis spectra of the thin films were recorded by spin coating the ZP-P4VP on quartz slides. Similarly, ATR-IT spectra were recorded by spin coating the polymer on top of quartz slides. NMR was recorded in $CDCl_3$ using TMS as internal standard. AFM images were obtained from ZP-P4VP spun silicon wafers. SEM images were obtained by coating gold on top of the thin films to avoid charging by the electron beam.

Fig. S1. Cartoon showing small molecules phase segregate at air polymer and polymer substrate interfaces, while blending with insulating vinyl polymers.

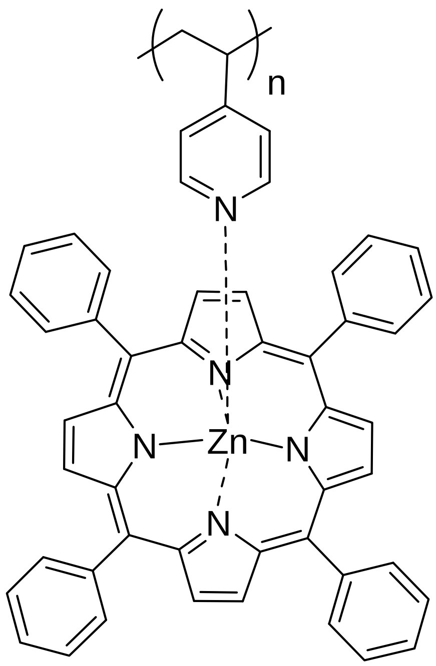

Fig. S2. Structure of zinc porphyrin forming penta coordinate complex with P4VP vinyl polymers.

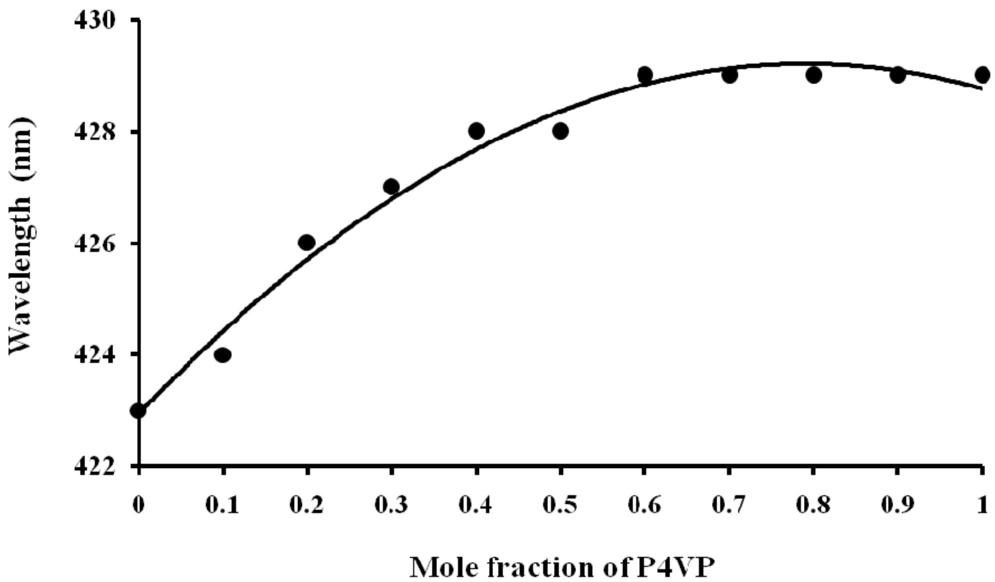

Fig. S3. Job's plot for quantitative determination of ZP and P4VP binding.

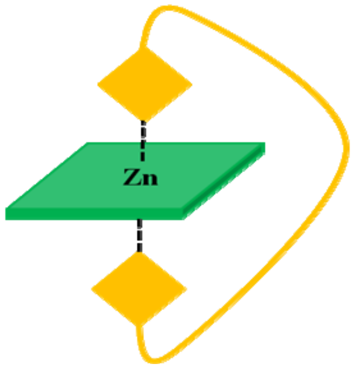

Fig. S4. Cartoon showing dynamic two-point binding between ZP and P4VP.

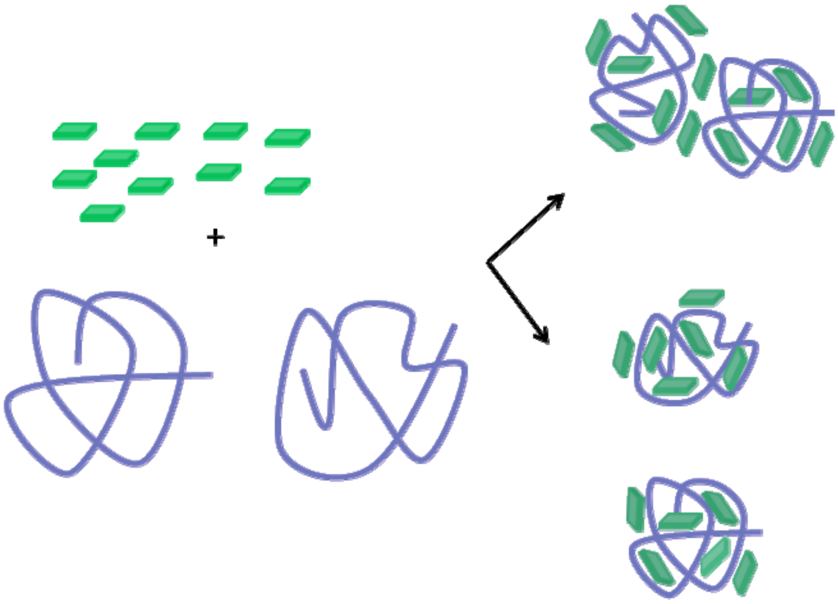

Fig. S5. Cartoon showing possible binding modes of ZP and its impact on the hydrodynamic diameter of P4VP.

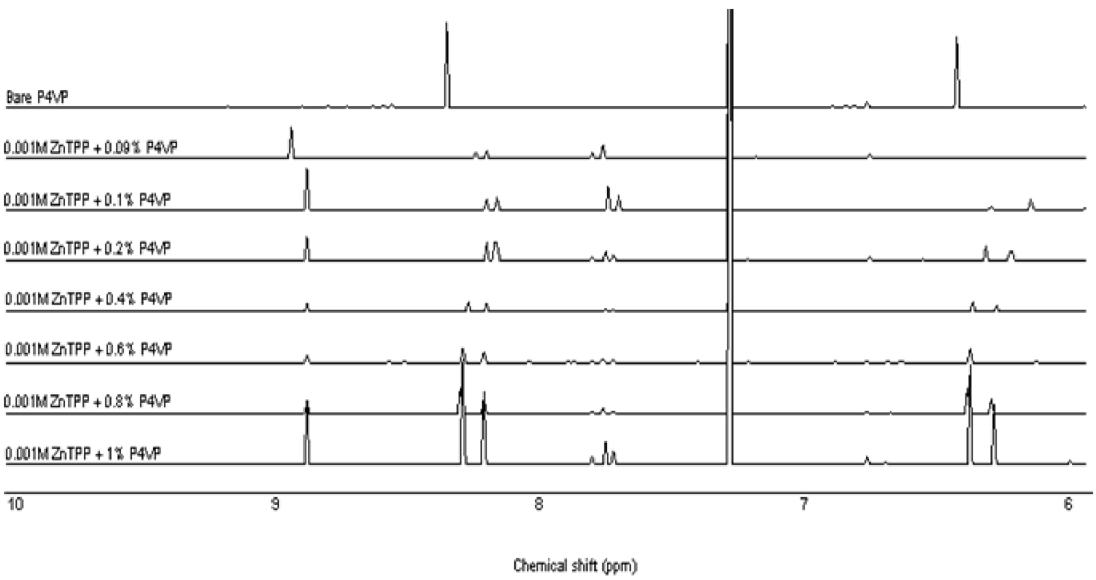

Fig. S6. NMR spectra showing the binding between ZP and P4VP.

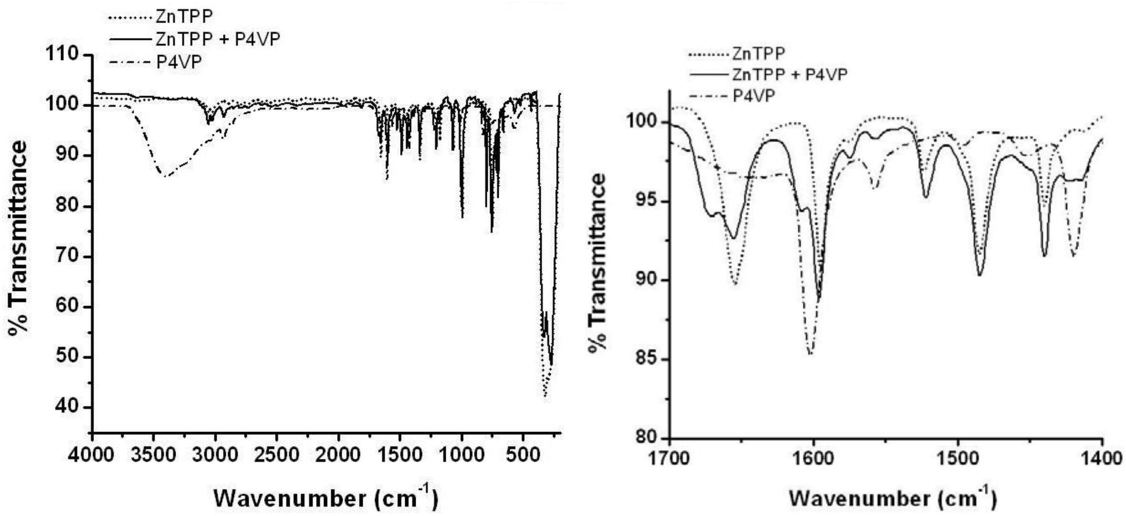

Fig. S7. ATR IR spectra of P4VP and ZP-P4VP supramolecular complex

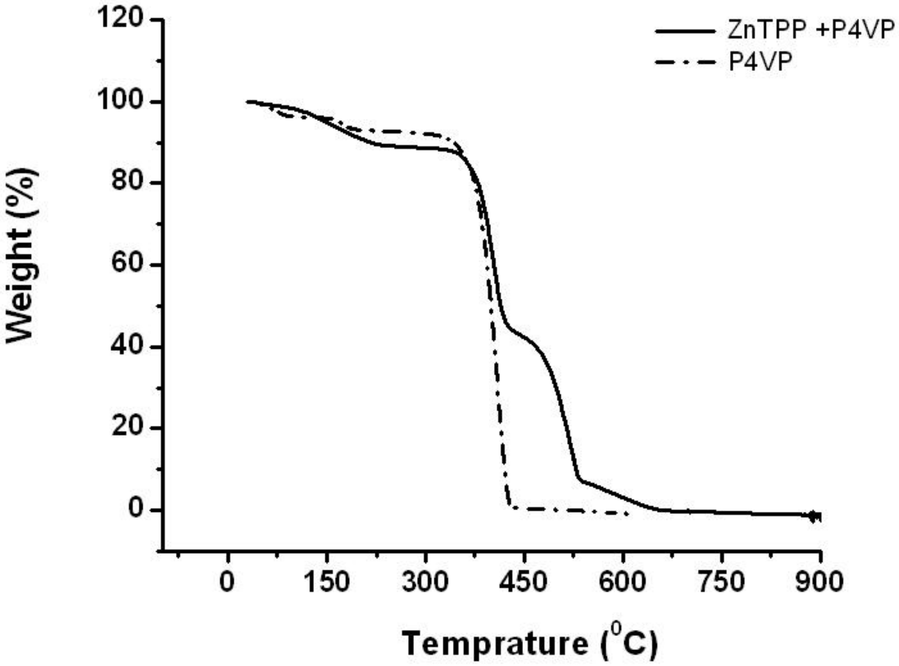

Fig. S8. Thermo gravimetric analysis curve showing percentage weight loss as a function of temperature for P4VP and ZP-P4VP.

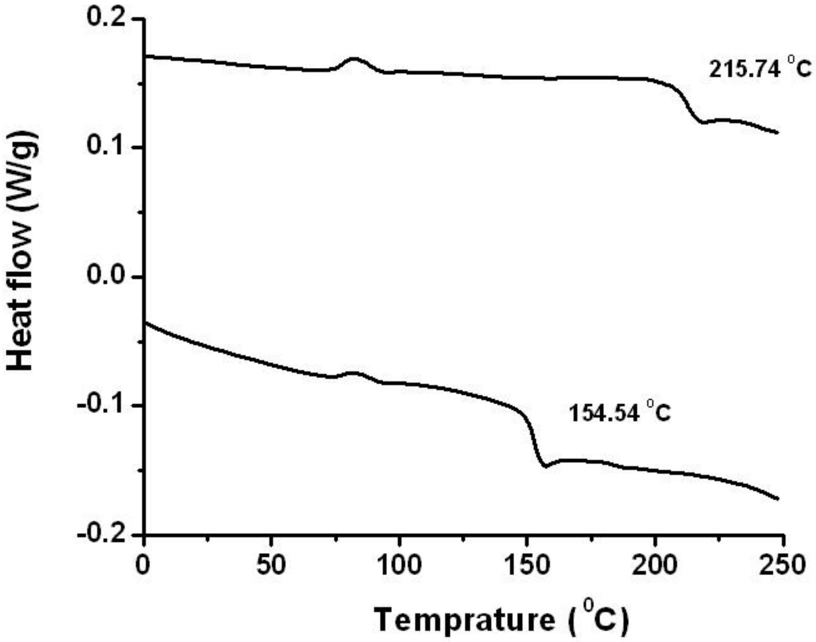

Fig. S9. Differential scanning calorimetry curves showing the *Tg* of P4VP and ZP-P4VP

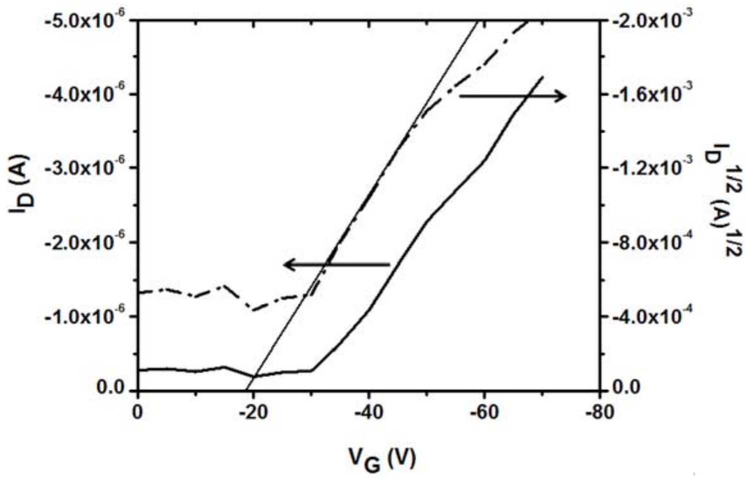

Fig. S10. Transfer characteristic I-V curves of ZP-P4VP measured at atmospheric condition without thermal annealing. The channel width and length was 10 mm and 5μm, respectively.

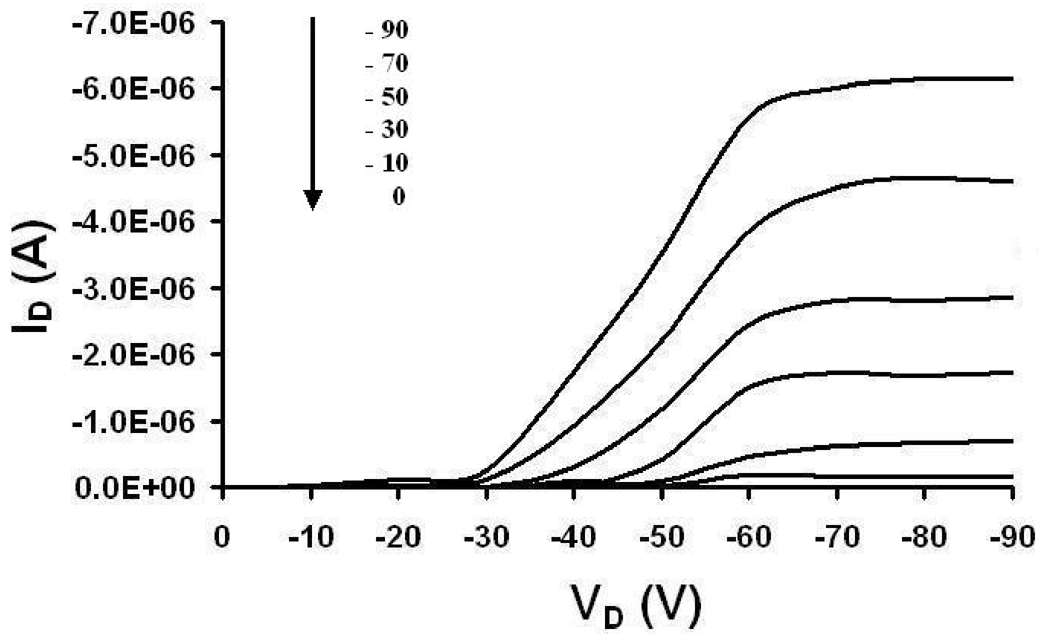

Fig. S11. Output characteristic I-V curves of ZP-P4VP thin film thermally annealed at 50° C.

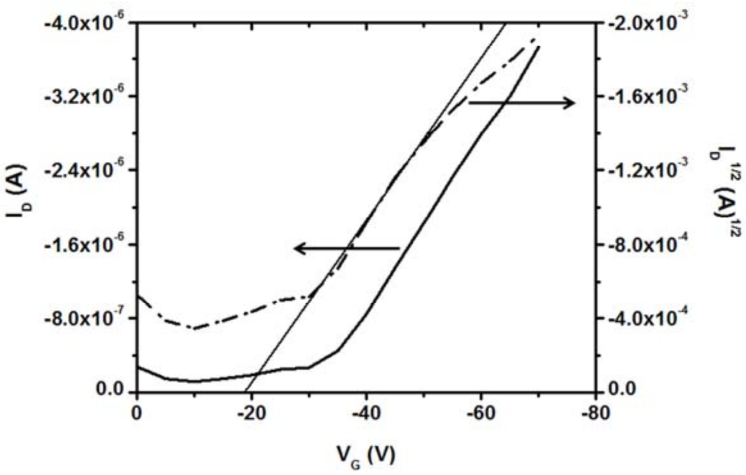

Fig. S12. Transfer characteristic curve of ZP-P4VP film annealed at 50° C.

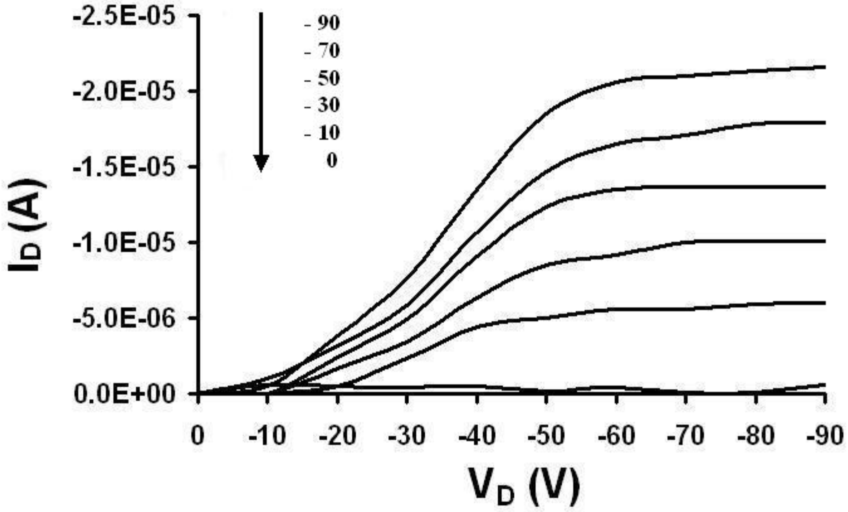

Fig. S13. Transfer characteristic curve of ZP-P4VP film annealed at 80° C.

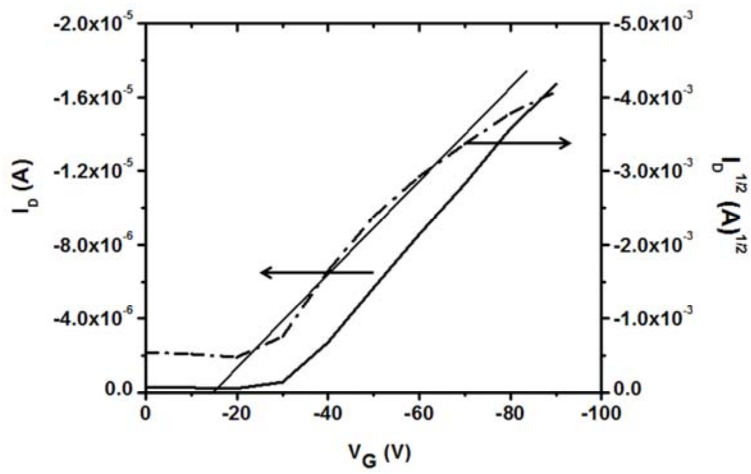

Fig. S14. Transfer characteristic curve of ZP-P4VP film annealed at 80° C.

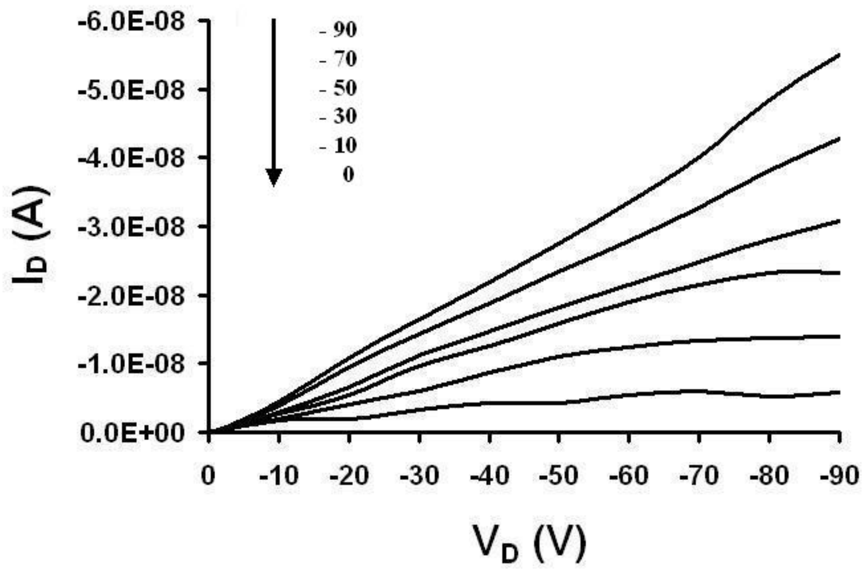

Fig. S15. Output characteristic I-V curves of ZP-P4VP thin film thermally annealed at 120° C.

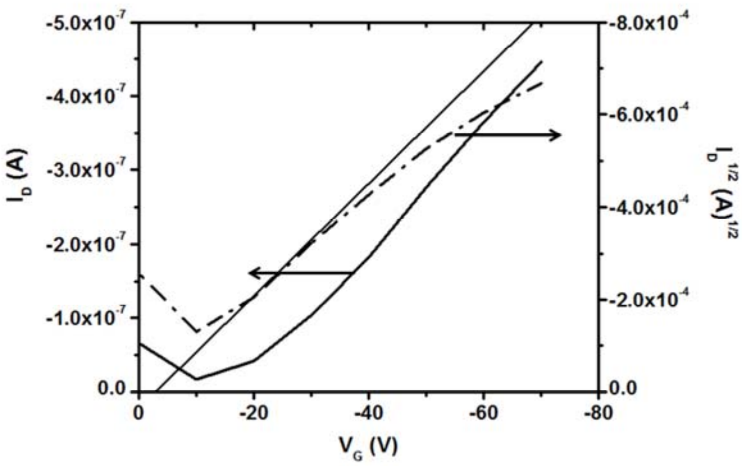

Fig. S16. Transfer characteristic curve of ZP-P4VP film annealed at 120° C.

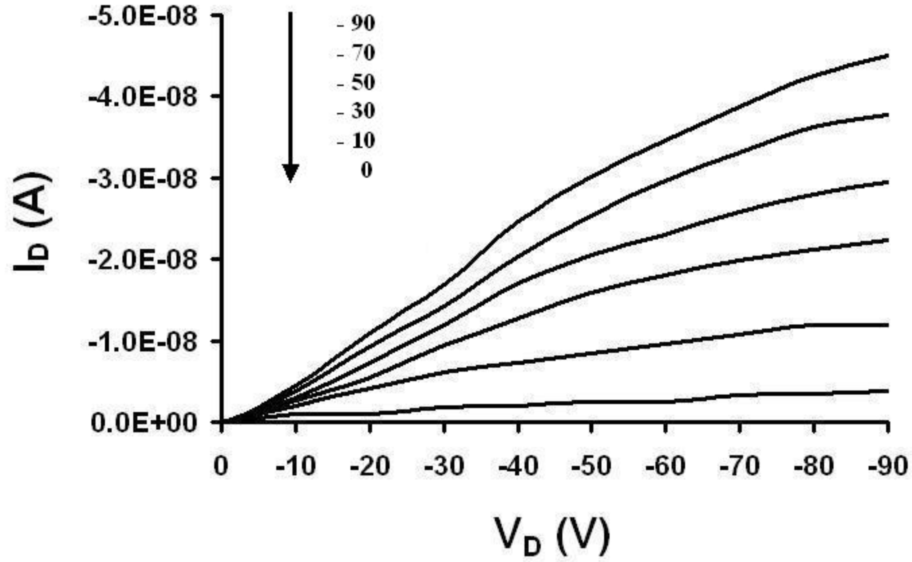

Fig. S17. Output characteristic I-V curves of ZP-P4VP thin film thermally annealed at 150° C.

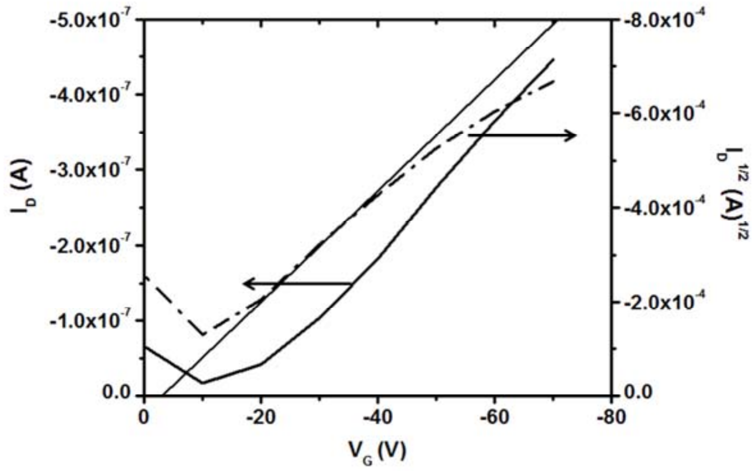

Fig. S18. Transfer characteristic curve of ZP-P4VP film annealed at 150° C.

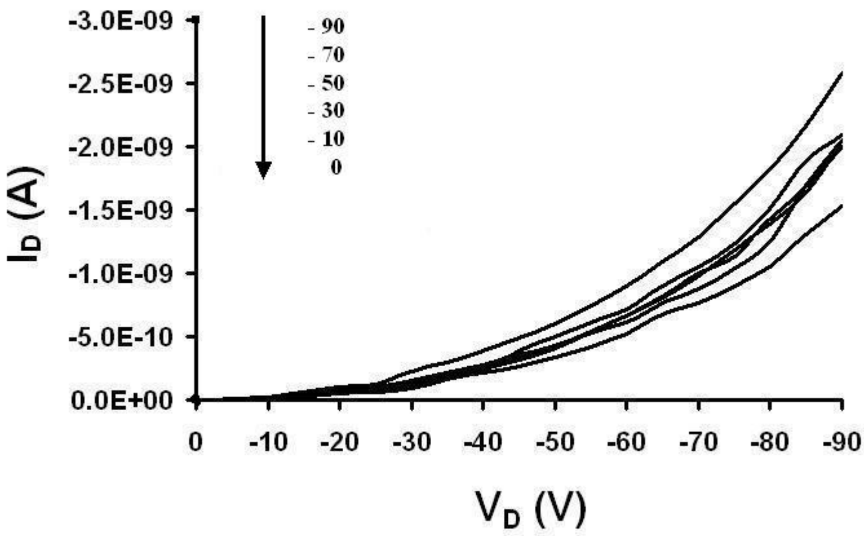

Fig. S19. Output characteristic I-V curves of ZP-P4VP thin film thermally annealed at 220° C.

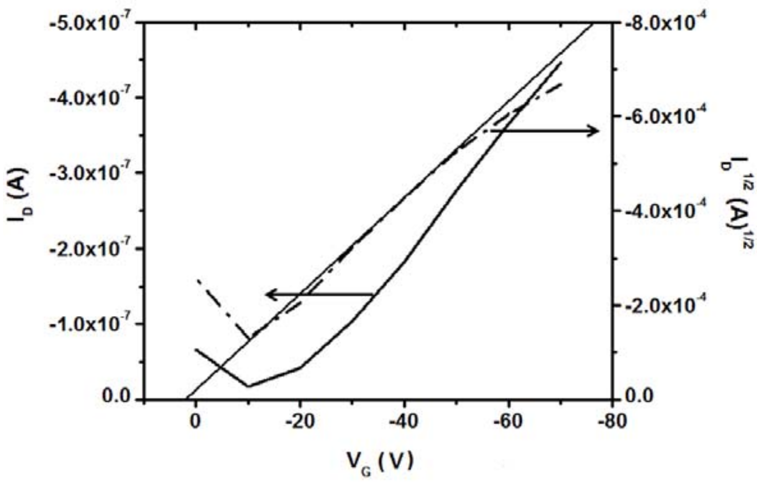

Fig. S20. Transfer characteristic curve of ZP-P4VP film annealed at 220° C.

Electronic Supplementary Material (ESI) for Polymer Chemistry

(a) (b)

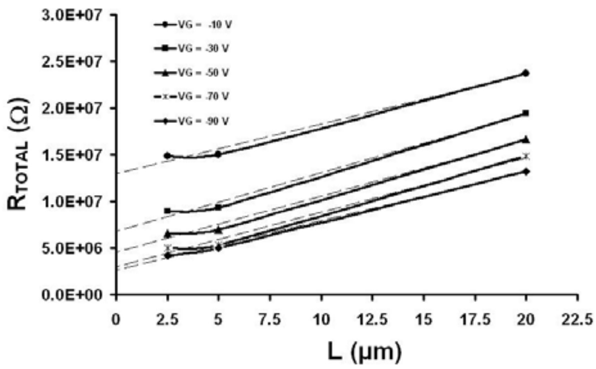

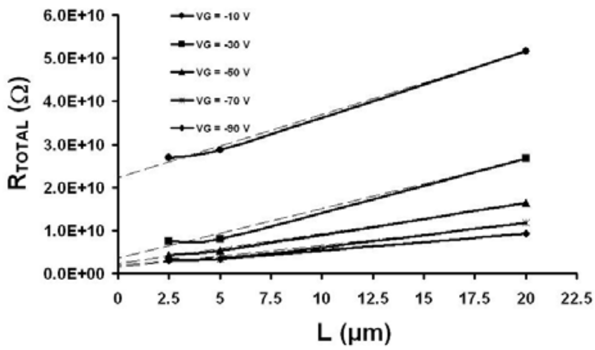

Fig. S21. Total resistance (RT) as a function of channel length (L) for ZP-P4VP film annealed at 80° C (a). Total resistance (RT) as a function of channel length (L) for ZP-P4VP film annealed at 150° C (b).

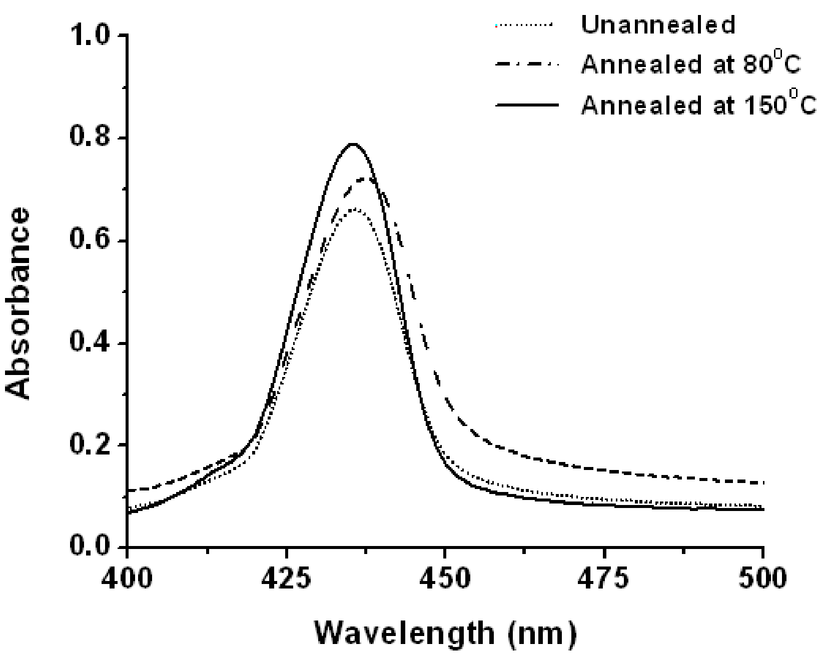

Fig. S22. UV-vis absorption spectra of ZP-P4VP films coated on quartz slide as a function of thermal annealing.

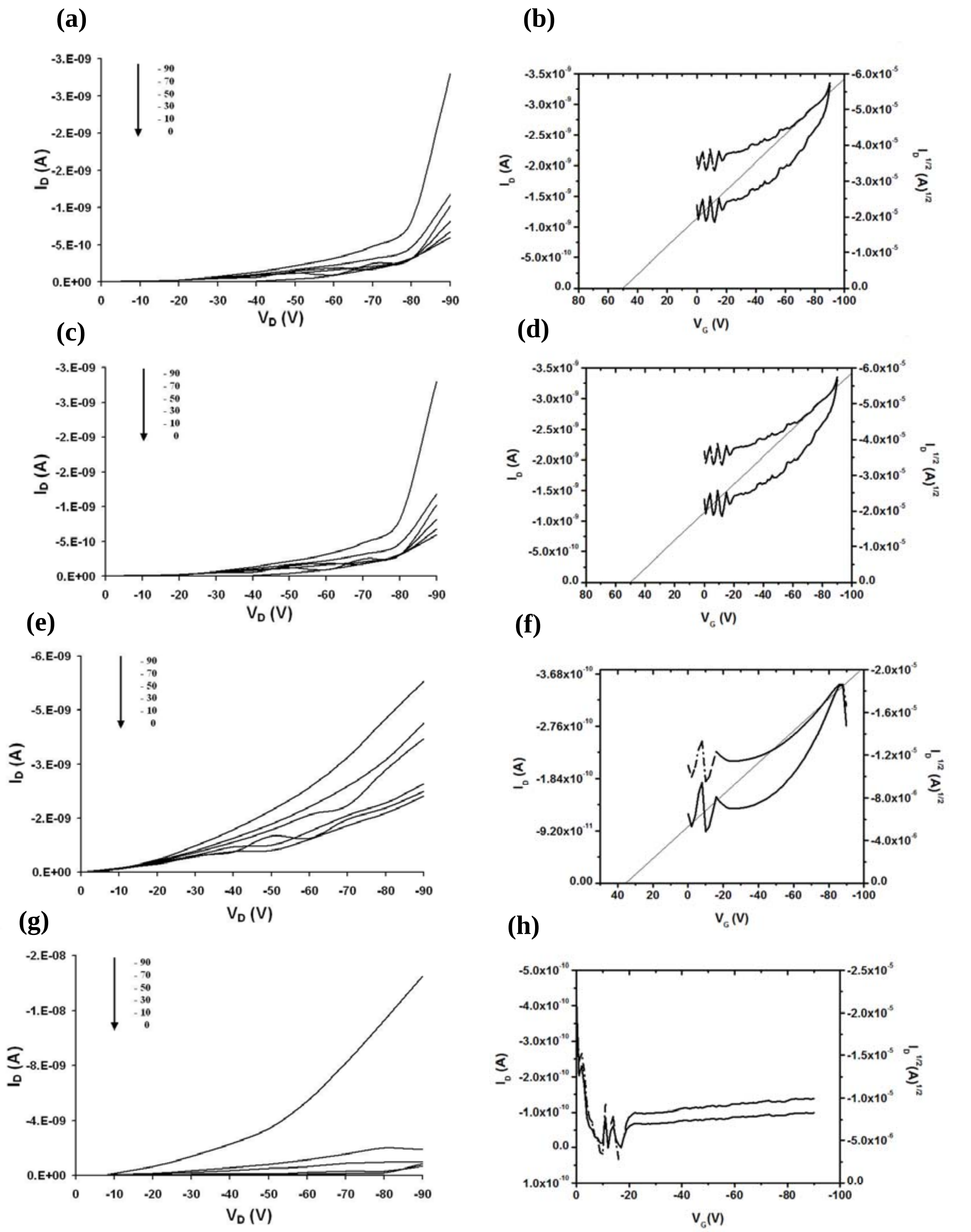

Fig. S23. Ouput and transfer characteristics of ZnTPP measured at 25°C (a and b), 50°C (c and d), 80°C (e and f) and 120°C (g and h).

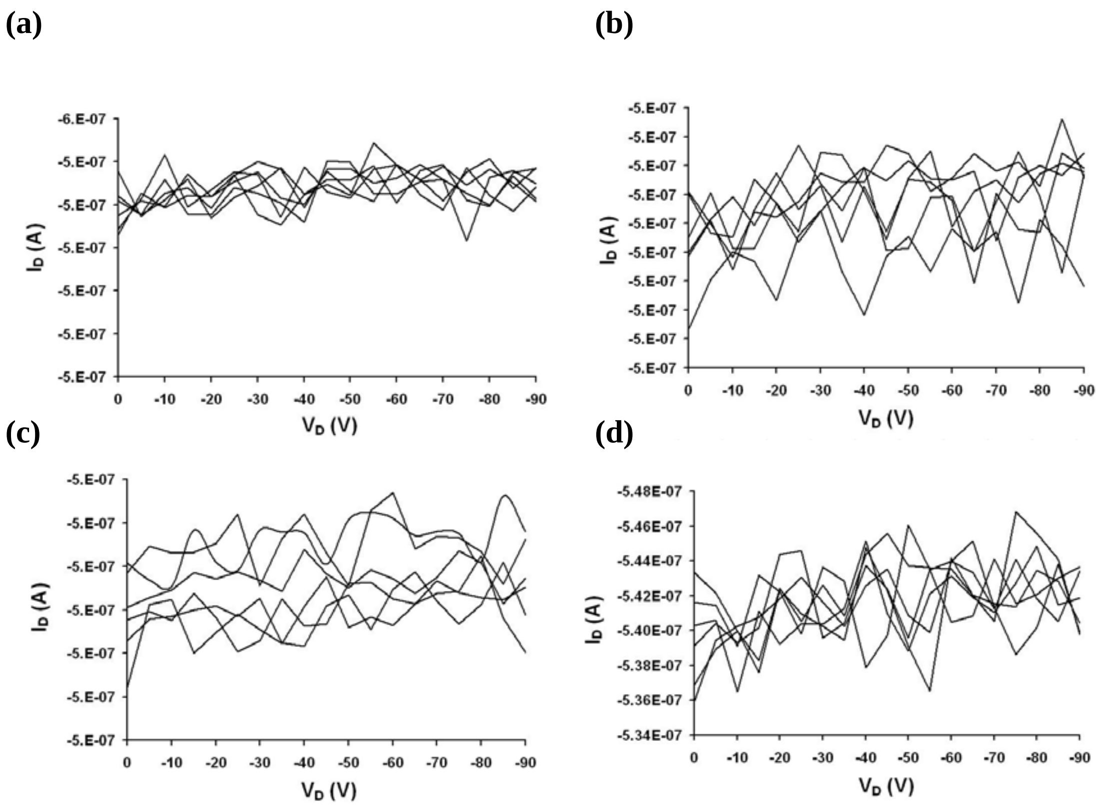

Fig. S24. Output characteristics of P4VP measured at 25°C (a), 50°C (b), 80°C (c) and 120°C (d).

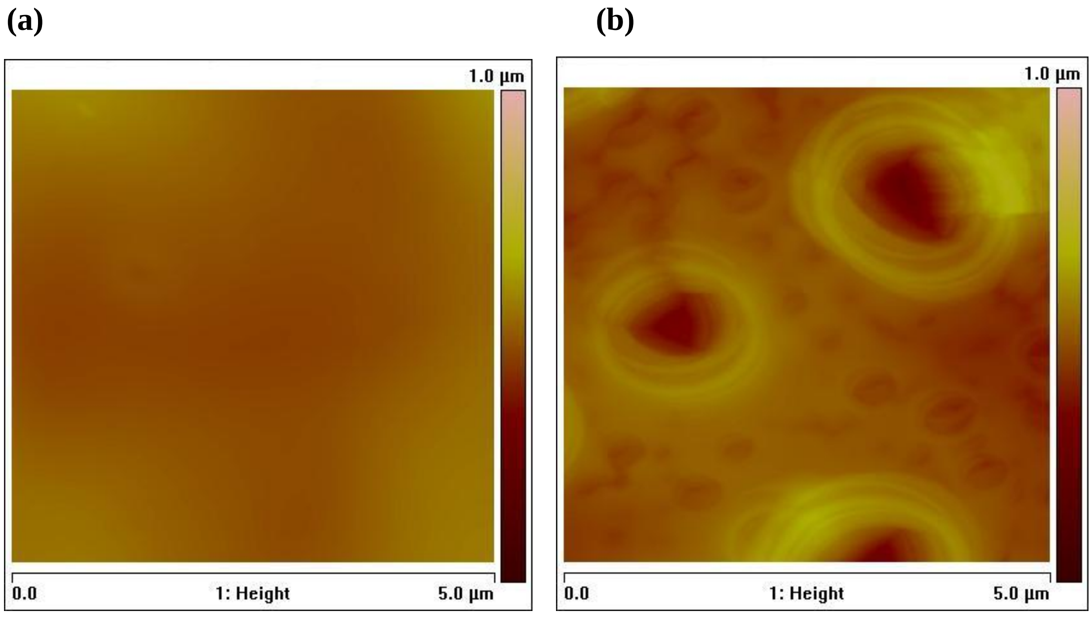

Fig. S25. AFM images showing surface topography of ZP-P4VP before thermal annealing and after thermal annealing at 220° C .

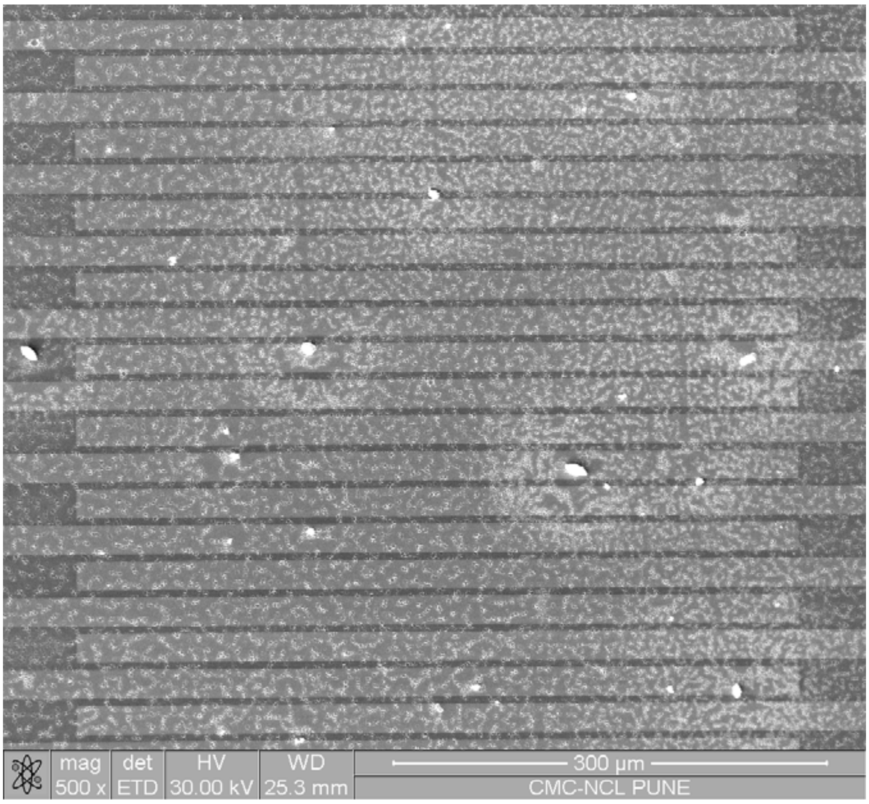

Fig. 26. SEM image of FET coated with ZP-P4VP annealed at 150° C. The micron size pores can be seen throughout the film.